Mars Global Surveyor: Aerobraking with a Broken Wing

by

Dr. Daniel T. Lyons
Jet Propulsion Laboratory, California Institute of Technology
4800 Oak Grove Drive, Pasadena, CA 91109
daniel.t.lyons@ jpl.nasa.gov
(81 8) 393-1004

ABSTRACT:

The Mars Global Surveyor (MGS) spacecraft was launched successfully on November 7, 1996 on a Delta II 7925. During the initial spacecraft deployment, one of the two solar wings failed to deploy far enough to latch into place. The unlatched configuration was a serious problem because Mars Global Surveyor will use an aerobraking phase much like that used to circularize the orbit of the Magellan spacecraft at Venus. The solar wings supply most of the surface area that provides the drag that will result in a total AV of more than 1200 m/s during the four month aerobraking phase. Aerodynamic moments at the unlatched hinge can be larger than 500 in-lb. Since the 60 in-lb spring force which is holding the unlatched panel in position for the planned aerobraking configuration is clearly not enough, a new configuration had to be developed for the aerobraking phase. This paper will describe the redesigned aerobraking phase, which will begin on September 17, 1997 3 orbits after a 980 m/s propulsive maneuver captures the MGS spacecraft into a 45 hour, 300 km periapsis altitude orbit around Mars on September 12, 1997 (01 :26 UTC).

THE MARS GLOBAL SURVEYOR SPACECRAFT

The Mars Global Surveyor spacecraft was designed to map the surface of Mars using instruments that were spares from the Mars Observer mission. The names of the instruments, principal investigators and primary purpose are listed in Table 1, Except for the magnetometer sensors, which are located at the outermost tips of the outboard solar panels, all of the instruments are located on the nadir panel, which is located on the +Z side of the spacecraft. During the mapping phase, which begins shortly after the spacecraft achieves a nearly circular 400 km Sun-synchronous orbit around Mars at the end of the aerobraking phase, the +Z-axis will be continuously pointed at nadir. The inner panel gimbals will rotate the two solar wings about the Y-axis (which will be orthogonal to the orbit plane) to maintain power, The panels will unwind during the eclipse that occurs every orbit for the 2 pm mean local solar time mapping orbit.

Mars Global Surveyor plans to use an aerobraking phase[1-5] that is very similar to the one pioneered by Magellan at Venus[6-8]. During the aerobraking phase that precedes mapping, the High Gain Antenna will remain stowed with the boresight pointed along the +X-axis. Figure 1 shows the spacecraft in the aerobraking configuration that was planned prior to launch. (The blankets that cover the propulsion module are not shown,) The atmospheric flow direction relative to the spacecraft is in the +Z direction, so the atmospheric molecules hit the propulsion module. The bipropellant engine is located along the centerline of the vehicle and provides 650 N of thrust along the +Z direction when the spacecraft is propulsively captured into a 45 hour orbit around Mars. The bipropellant main engine will also be used for all of the larger trajectory correction and orbit trim maneuvers, which means that the High Gain Antenna cannot be deployed until after the last bipropellant maneuver, because the deployed position is located in the exhaust plume near the -Z axis. During mapping, the High Gain Antenna will be gimballed to point at the Earth, except during unwinds. Attitude control is provided by 4 reaction wheels and by 12 (4.45 N) thrusters, which are located at the ends of the "feet" that stick out near the bottom (-Z) end of the spacecraft.

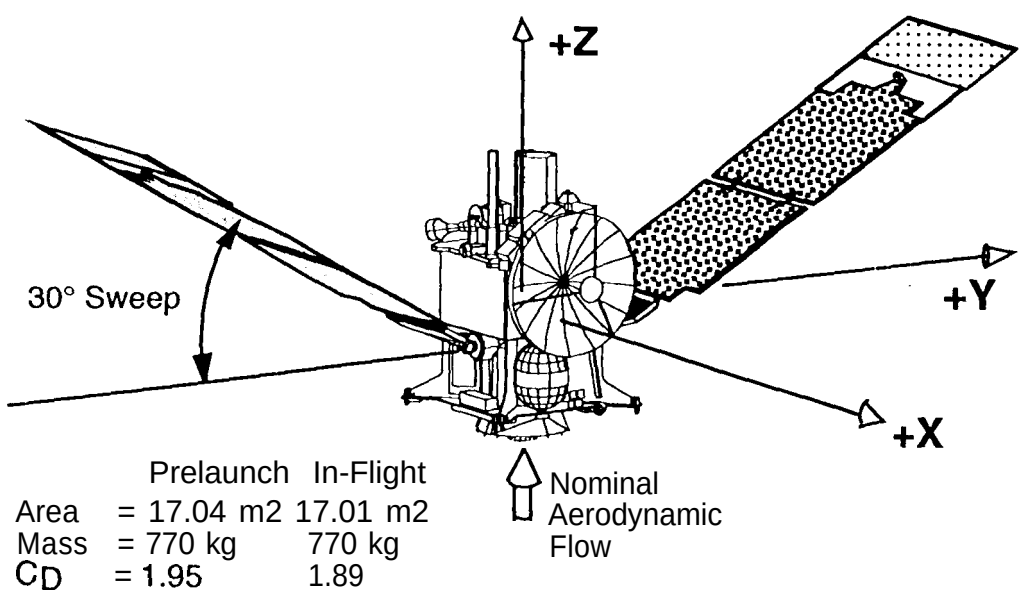

Figure 1: The Aerobraking Configuration with Fully Deployed Solar Wings.

A BRIEF HISTORY

The Mars Global Surveyor spacecraft was launched successfully on November 7, 1996 on a Delta II 7925. During the initial spacecraft deployment following launch, one of the two solar wings failed to deploy fully. The solar array has two wings, one on each side of the spacecraft. The spacecraft axes are shown in Figure 1, which shows the planned configuration for aerobraking with the solar

Table 1: Instrument Names and Purpose

Acronym	Full Name	Principle Investigator and Home Institution	Objective
Mag/ER	Magnetometer and Electron Reflectometer	M.H. Acuna Goddard Space Flight Center (GSFC)	Intrinsic magnetic field and solar wind interactions with Mars
MOC	Mars Orbiter Camera	M.C. Malin Malin Space Systems (MSSS)	Surface and atmospheric imaging
MOLA	Mars Orbiter Liner Altimeter	D.E. Smith Goddard Space Flight Center (GSFC)	Surface topography and gravity field studies
MR	Mars Relay Radio System	J. Blamont Centre Nationale d'Estudies Spatiales (CNES, France)	Relay Support for future Mars Lander missions, both American and International
TES	Thermal Emission Spectrometer	P.R. Christensen Arizona State University (ASU)	Mineralogy, condensates, dust, thermal properties, and atmospheric measurements
USO (RS)	Ultra Stable Oscillator for Radio Science	G.L. Tyler Stanford University (team leader)	Gravity field determination and atmospheric refractivity profiles

wings fully deployed, Figure 2 shows that each wing has two solar panels, which are joined by 2 spring loaded hinges. A deployable kapton flap is mounted to the outer end of the outer panel for added drag during the aerobraking phase. The inner panel is attached to a "Y shaped yoke by two spring loaded hinges and a damper. The yoke is attached to the 2-axis gimbal which is mounted on the spacecraft bus. To achieve the launch configuration, each wing was folded by almost 180° at the yoke-to-panel and the panel-to-panel hinge lines, with the flap sandwiched in between the two panels. The gimbals were rotated to put the yoke almost flat against the side of the spacecraft so the vehicle would fit inside the shroud. (The notches in the corners of the panels allowed the adjacent part of the panel and magnetometer extension to stick down between the thruster modules in the launch configuration.)

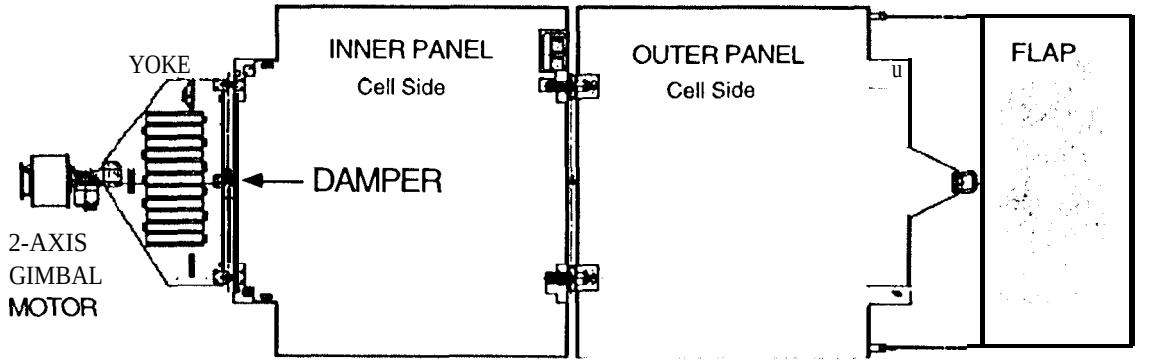

Figure 2: A Solar Wing

After launch, the +Y wing deployed fully and both of the panels latched into place such that the yoke, panels, and flap all were in the same plane as shown in Figure 2. The cell side of the panel is on the same side as the shunt radiators, which are mounted on the yoke as shown in Figure 2. The hinge between the outer and inner panels on the -Y wing latched into place and the flap deployed, so the panels and flap all lie in the same plane. Unfortunately, the hinge between the inner panel and the yoke assembly did not latch into place.

Telemetry from the sun sensor mounted on the inner panel indicated that the hinge between the yoke and the inner panel was 20.5° away from full deployment. Imagine the panels in Figure 2 lying flat on a table with the cell sides up, The unlatched yoke would be angled up from the table by 20.5°. “Wiggle tests” using the gimbal motors to shake the -Y-wing showed that the hinge is not latched, The failure scenario that explains both the body rates during deployment and which is consistent with a 20.5° offset is that the deployment damper shaft sheared off during deployment at about the time when the outer panel snapped into place which allowed the damper arm that turned the shaft to become wedged between the inner panel and the yoke.

Figure 3 shows an expanded view of the damper assembly, which is located at the midpoint of the hingeline between the yoke and the inner panel. Figure 3 illustrates three positions during deployment: launch, partially deployed and the position where the damper arm is in contact with both the yoke and the inner panel. One end of the damper arm was supposed to remain fastened to the square end of a shaft through the center of the damper mechanism, while the other end was, and still is, loosely pinned to the inner panel. During deployment, the

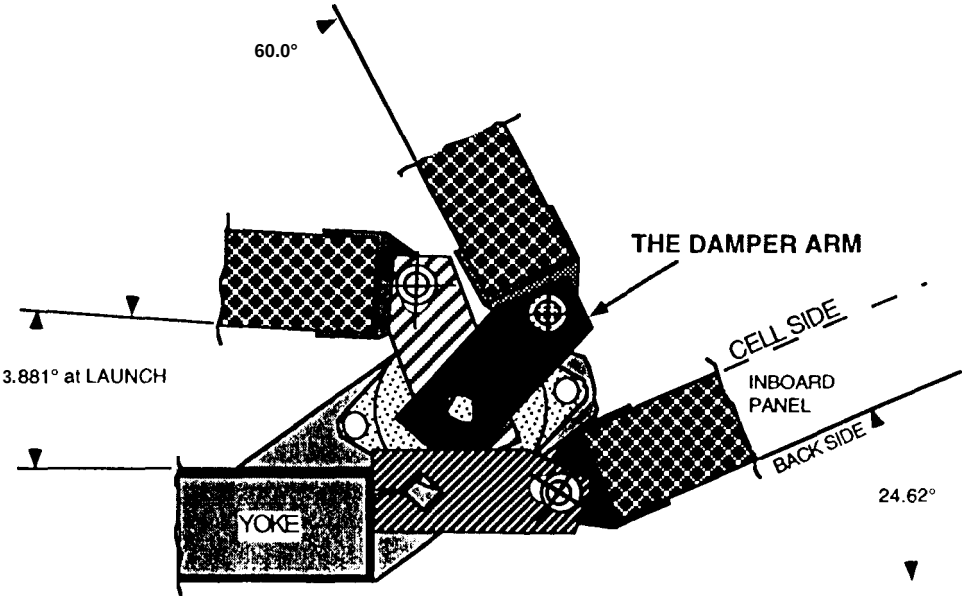

Figure 3: Damper Arm Location at 3 Points During Deployment

spring loaded hinges pushed the panel away from the yoke (launch configuration), which caused the shaft to rotate and move a paddle on the inside of the damper through a viscous fluid to slow the rate of deployment in order to reduce the shock on the gimbal when the panel snapped into place. There was no damper between the inner and outer gimbal panels, so the outer panel snapped into place much more quickly, and with more force than the inner panel. Figure 3 shows that the undeformed geometry would result in a 24.6° offset angle, however, one end of the damper arm has a sharp point, which is believed to have penetrated a very short distance into the bracket attached to the inboard panel enough for the panel to reach 20.5° from full deployment. The location of the cell side of the panel is on the inside of the "V", and the springs are trying to open the "V".

The deployment springs, which are currently supplying a moment of about 60 in-lb, are enough to hold the panel in position during most of the mission. The planned propulsive maneuvers using the main engine would have applied a moment of about 300 in-lb about the hinge, so the spacecraft team had to reconfigure the spacecraft for propulsive maneuvers so that the propulsive acceleration would generate a moment orthogonal to the hinge rather than around the hinge as originally planned. The first Trajectory Correction Maneuver demonstrated that the new configuration would work for high thrust maneuvers. Each pass through the atmosphere will produce approximately 600 in-lb of torque at the hinge. If the aerodynamic force pushed on the backside of the unlatched wing, which is desired for the fully latched configuration, then the panel would push against the spring, which cannot hold the panel in the desired configuration and the hinge would "collapse". The cross sectional area with a collapsed panel would be too small to achieve the desired drag, not to mention the possibility that the panel could crash into the spacecraft causing physical damage, or the certainty that the changing aerodynamic characteristics would require excessive propellant to maintain attitude control.

The new configuration shown in Figure 4 was developed for the aerobraking phase. The velocity vector during the drag pass is still along the -Z axis, which means that the atmospheric molecules hit the panels on the side that is visible in

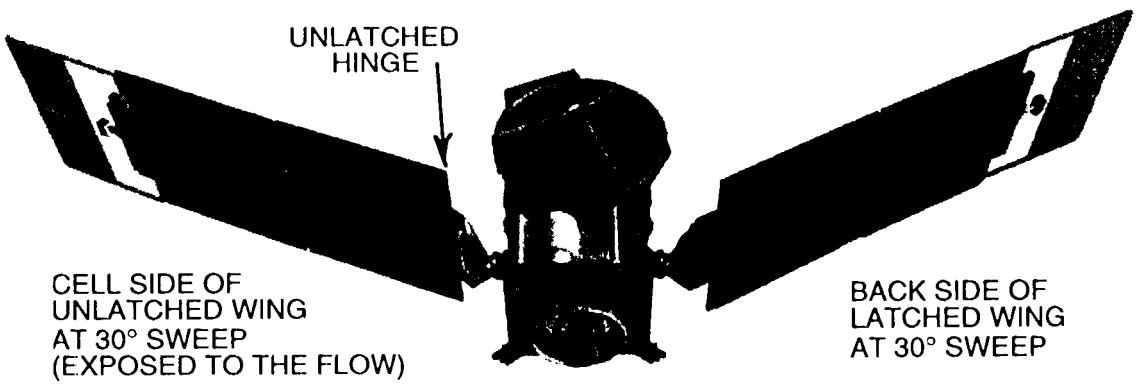

Figure 4: The New Aerobraking Configuration

Figure 4. The fully latched +Y wing (on the right) isin the same configuration as before, with the back side of the panel exposed to the flow. Starting from the originally planned configuration shownin Figure I, the unlatched -Y wing has been rotated 180° around the inner gimbal (about the Y-axis) and then rotated from the hardstop at 30° by 80° (2 • 30° + 20° for the kink at the unlatched hinge) around the outer gimbal (parallel to the hinge line) in order to achieve the configuration that is aerodynamically almost the same as the fully latched configuration.

DIFFERENCES BETWEEN LATCHED AND UNLATCHED CONFIGURATIONS

There are three very important differences between the fully latched configuration and the new configuration. The first difference is that the solar cells are exposed to the flow. The side of the panel that is exposed to the flow runs about 40° C hotter than the other side of the panel, which means that the cells will get hotter than planned and will go through a larger amplitude thermal cycle every orbit for the new configuration. The qual panel was retested in the thermal vacuum chamber to demonstrate that the cell sides of the panels could withstand higher temperatures (165° C) for many cycles. In fact, none of the cells on the qual panel showed any change in power output even after being heated to the maximum temperature that could be achieved by the chamber (1 92° C) for several cycles. During the pre-launch acceptance test at 165°C, many cells on the flight panels were damaged, so the panels had to be repaired and retested. Although the qual panel survived at 192°C, there is still some concern that there may be differences in the thickness of the adhesive between the qual and the flight panels which could result in damage to some of the flight cells at lower temperatures than for the qual panel. Thus, the 165°C acceptance test temperature will be used to set the flight allowable limits, even though the post launch test show that the panels would probably survive much higher temperatures. A detailed thermal analysis of the components at various locations on the panel at various times during aerobraking resulted in a request for waivers for several non-critical components, like the Sun-sensor in order to achieve an acceptably high flight allowable temperature. (There are several other Sun-sensors that are in more protected locations.)

The second difference between the original and the unlatched plans is that the outer gimbal must be powered on during the drag pass in order to hold the unlatched panel in position. The unpowered gimbal holding torque is insufficient to guarantee that the panel will not backdrive the gimbal. The latched configuration does not require the gimbal to be powered on, because there is a hard stop at the nominal 30° sweep position in that direction. (The other hard stop is at nearly 90° when the yoke is parallel to the body for the launch configuration.) The gimbal will overheat if left in powered hold mode for the entire orbit, so the aerobraking block that specifies the sequence of events during the drag pass had to be modified (and retested) to turn the gimbal on at the start of a drag pass, and off at the end. The contractually specified 600 in-lb holding torque of the gimbal motor was just barely enough to hold the panel in position when the atmospheric density was close to the

value that would overheat the panel, but the maximum actual holding torque was unknown. The gimbal manufacturer tested a similar gimbal assembly at double the specified maximum in order to demonstrate that the powered gimbal would be able to hold the panel in position with an adequate design margin.

Although the unlatched panel is positioned to achieve the same aerodynamic configuration as the original plan, an option to use the gimbal to maximize the area by placing the panel close to the -Y axis, rather than swept back by 30°, was considered. Such a configuration would reduce the peak heating rates because the spacecraft could fly at a lower density and still achieve the required ΔV, but the torques on the gimbal motors would be slightly higher. At the time this option was being considered, the gimbal torques were a greater concern than the heating rate, so it was never studied thoroughly. The very tight redesign schedule required the amount of analysis to be minimized. Since the current plan appears to have adequate thermal margin, other options were unnecessary.

The third difference between the original and the unlatched plans is that the unlatched panel is not as stiff as the latched panel. In the new configuration, the aerodynamic force on the cell side of the panel will push the panel against the broken damper arm, The stiffness of the obstruction was characterized by using the gimbal motor to “Wiggle” the unlatched wing back and forth at the natural frequency. Comparing body rate telemetry to various models showed that the panel was characterized by the 60 in-lb deployment spring in one direction and by a very stiff, non-linear spring in the direction of the obstruction. (Torque $\approx$ 1300 in-lb/radian $\bullet X^{1.3}_{\text{Radians}}$) During a typical drag pass, the panel is expected to deflect by about 10°, which will change the aerodynamic null attitude by about 5°. Fortunately, the deadband of the control system is 15° during the drag pass, so the deflection is not enough to trigger unnecessary thruster activity.

Figure 5 shows Attitude Errors from an AACS simulation of a typical drag pass for the new configuration for a 24 hour orbit period with average initial conditions. The error is measured relative to the polynomial reference attitude which is trying to point the +X axis at nadir and the Y-axis orthogonal to the orbit plane during the drag pass. The error about the Y-axis (lower curve) goes through almost 6 oscillations in 300 seconds. The spacecraft oscillates (by $\pm 2°$) about a mean value of -7° because the simulation included a timing error which is equivalent to a bias about the Y-axis. (The goal is to keep the timing errors smaller than 225 sec to keep this bias inside the deadband of the control law.) The curve which starts near zero, reaches a maximum value of about 5° and then returns to within 10 of zero is the error about the X-axis. The X-axis oscillation has a higher frequency (9 cycles in 300 see) and a smaller amplitude (*10, because the aerodynamic moment about the X-axis is larger than that about the Y-axis. The hump in the middle of the X-axis error is due to the panel deflection, which is a maximum near periapsis where the aerodynamic forces and deflections are largest. The only difference between the unlatched and latched simulations is this hump in the X-axis aerodynamic null attitude. The other aspects of the simulation

are the same whether the wings are latched or unlatched. The X-axis error is “out of the orbit plane” and is insensitive to timing errors. The remaining curve, which starts at zero and increases steadily for most of the drag pass is the Z-axis error. The plot shows the position error after it has been filtered by the control system limit logic. The sharp decrease at about 350 seconds from the start of the simulation represents a change in the AACS control parameters to “tighten” the dead band to reduce the residual body rotation rate before switching back to reaction wheel control at the end of the drag pass.

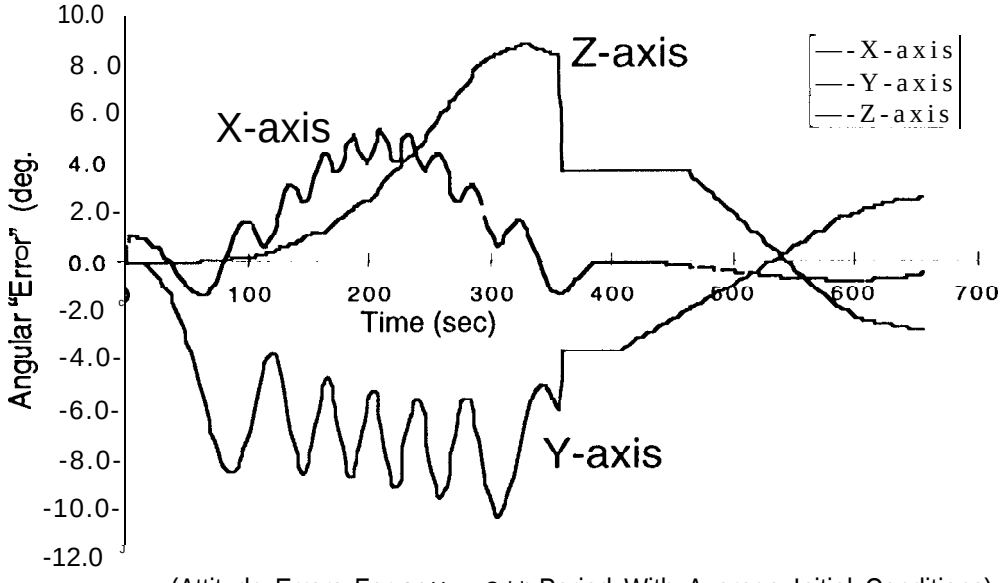

(Attitude Errors For 24 Hour Orbit Period With Average Initial Conditions).

Figure 5: AACS Simulation of a Typical Drag pass with New Configuration

SEQUENCE OF EVENTS DURING AN AEROBRAKING ORBIT

Figure 6 shows the sequence of events during a typical aerobraking orbit. The only changes to the sequence due to the unlatched solar wing are that the -Y solar wing gimbal is put into powered hold mode at the start of the drag pass and taken out of powered hold mode at the end of the drag pass. (The -Y gimbal angles are different, but the process of positioning the panel for the drag pass is nearly the same as originally planned.)

Figure 6 also shows several things which do not occur on every orbit. For example, eclipse from the Sun only occurs near the end of aerobraking. At about the time the spacecraft begins to experience power loss due to eclipse, the science instruments will probably be turned off to maintain energy balance for the orbit, so it is unlikely that science playbacks will occur on the same orbit as an eclipse. The two playbacks of Science data and the post drag slew to take a MOC image will be eliminated when the instruments are turned off. Figure 6 also shows a propulsive maneuver at apoapsis which is used to raise or lower the periapsis altitude to control the amount of aerodynamic drag and heating for the next orbit. These propulsive maneuvers do not occur every orbit.

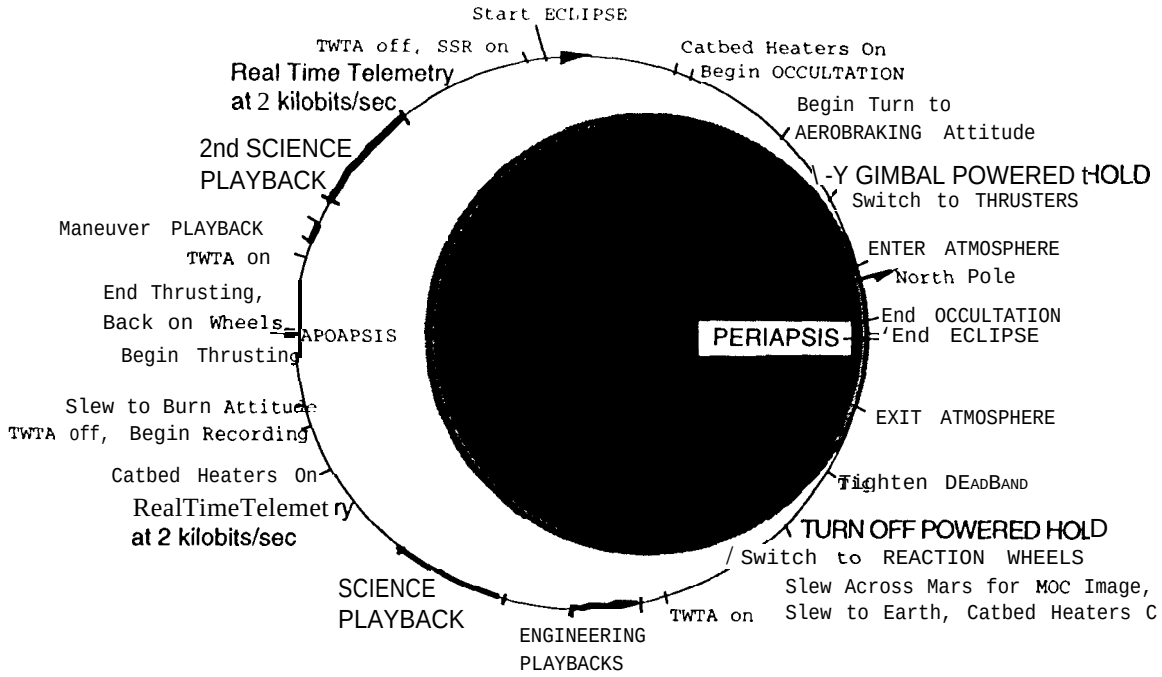

Figure 6: Typical Events inan Aerobraking Orbit.

For most ofthe orbit, the spacecraft is in Array Normal Spin mode, where the +X-axis (High Gain Antenna) ispointed at the Earth for telecom and the spacecraft is rotating vetyslowly about the X-axis (once every 100 minutes) to view stars with the star scanner and update the attitude knowledge. The sequencing subroutine (Aerobraking Block) that is called every aerobraking orbit begins about 30 minutes before periapsis (near thetopof Figure 6) when the catbed heaters are turned on. Afewminutes later, thespacecrafi changes attitude forthe drag pass. The +X-axis is pointed toward nadir and the Y-axis is oriented orthogonal to the orbit plane. The spacecraft also reorients the solar panels to the new aerobraking configuration shown in Figure 4, puts the -Y gimbal into powered hold mode to hold the solar wing against the aerodynamic moment, and then switches to thruster control mode with a wide deadband. If the Navigation team has predicted the time of the next periapsis perfectly, the spacecraft will enter the atmosphere (defined as a dynamic pressure of 0.0015 N/m*) 5 minutes later.

While passing through the atmosphere, the spacecraft will oscillate around the aerodynamic null, as was shown in Figure 5. A large control deadband of about 15° is used to minimize thruster activity while the spacecraft is in the atmosphere, since the aerodynamics will determine the attitude of the vehicle in spite of the thrusters. The spacecraft remains on thruster control for another 5 minutes following the expected exit from the atmosphere because the actual time of periapsis could be on either side of the predicted time. The deadband is tightened up soon after the expected exit from the atmosphere to damp out any residual rotation rates that were created by the aerodynamic forces before the spacecraft switches back to reaction wheel control.

During the larger period orbits where the science instruments are on, the spacecraft will slew around the Y-axis immediately after the drag pass in order scan the Mars Orbiter Camera (MOC) boresight across the planet and generate an image using the Wide Angle and Narrow Angle cameras. These images will be used to watch for dust in the atmosphere and for science. The spacecraft will then return to Array Normal Spin mode in order to recharge the batteries and regain communication with Earth. The batteries are partially discharged whenever the spacecraft is configured for the drag pass. The High Gain Antenna is not pointed toward the Earth during the drag pass, so all of the required engineering telemetry must be recorded on one of the solid state recorders for playback following the drag pass. One of the key pieces of information in this playback is the maximum panel temperature during the drag pass. If the panels are getting too hot, it is very important that a periapsis raise maneuver is triggered at the next apoapsis to reduce the density, and thus lower the heating rate for the next drag pass.

SCIENCE MEASUREMENTS IN SUPPORT OF AEROBRAKING

Since the Mars Global Surveyor mission is being flown with a very small flight team, the original plan was to leave the science instruments turned off until the mapping orbit was achieved because the spacecraft team would be too busy during the aerobraking phase to actively manage the instruments. Since the atmosphere will fluctuate from orbit to orbit, the design allowed for the atmospheric density to be twice the expected value without damaging the spacecraft. As the **design team learned more about the Martian atmosphere, it soon became obvious** that a factor of two was not enough margin to accommodate the density increase that accompanies a large global dust storm. Data from previous missions and software simulations of the Mars Atmosphere suggested that the density at the aerobraking altitude could increase by an order of magnitude in less than a week. In order to prevent damage in the event that a large global dust storm begins during the aerobraking phase, frequent real-time measurements of the atmosphere were required. Since several of the Mars Global Surveyor instruments are able to study the atmosphere, the project was willing to accept a more complicated operations phase in order to obtain data about the atmosphere from the science instruments to support the maneuver decision process during aerobraking operations.

The science data is recorded continuously during the orbit and played back in two segments. The first half of the science data is played back between 3 and 4 hours after periapsis, in time to provide data for the meeting to decide if a maneuver to raise or lower periapsis is needed at the next apoapsis. The second half of the data is played back a few hours after apoapsis, in time to provide data in case a last minute maneuver is required to raise periapsis three hours before the spacecraft reaches the atmosphere for the larger period orbits.

The most useful measurement is expected to be from the Thermal Emission Spectrometer (TES) because the atmospheric temperature can be inferred from the TES data between the surface and about 40 km. Since the nominal boresight (+Z) is orthogonal to the ANS spin axis (-X), and since the TES scan mirror moves the boresight orthogonal to the spin direction, it is possible make a very low resolution image of the planet once per spin, or every 100 minutes during Array Normal Spin. The TES will be able to detect rapidly changing atmospheric temperatures due to the rapidly increasing dust concentrations at the start of a global dust storm, (The dust is heated by the Sun and warms the surrounding atmospheric **molecules,** causing the atmosphere to expand and increase the densities at higher altitudes.)

The Mars Observer Cameras create images by moving the spacecraft such that a single line detector array moves across Mars. Although the boresight of the line array (+Z) is orthogonal to the spin direction, it is not possible to create images while in Array Normal Spin because the line array is parallel to the YZ plane and the spacecraft is rotating about -X, On the other hand, at the end of every drag pass the line array is oriented such that a slew about the Y-axis of the spacecraft will always scan the line array across Mars, which enables a single slew maneuver to be built into the sequence and run every orbit, which minimizes the intervention required by the operations team to collect the data, Minimizing the workload is absolutely necessary during this critical phase of the mission to keep the operations team from becoming exhausted. The MOC images should be able to confirm the TES measurements by detecting an increasing haze near the limbs as well as dust clouds near the nadir track.

A third science instrument, the electron reflectometer, can be configured as a Langmuir Probe, which will enable a measurement of the altitude of the electron peak during the drag pass through the atmosphere. The altitude of the electron peak will rise as the atmosphere expands during a global dust storm. It is not yet clear if the electron peak rises fast enough to enable the early detection of a global dust storm that is required to trigger a periapsis raise maneuver before the density doubles.

Three types of engineering telemetry can also be used to measure atmospheric properties. The accelerometers will be used to measure the drag on the spacecraft, which will be converted into densities and scale heights by using calculated drag properties. One of the four horizon sensor quadrants will see Mars during the drag pass. This measurement is similar to the TES measurement, only it is not as sensitive, nor does it provide as much coverage of the planet, The main use will probably be during the end of the aerobraking phase, when the science instruments will be turned off to maintain a positive energy balance. The final engineering measurements that provide information about the atmosphere are the temperature sensors on the solar wings. Higher densities will result in hotter temperatures.

The Mars Pathfinder spacecraft landed successfully on Mars on July 4, 1997. If the Pathfinder spacecraft survives beyond the prime mission, which ends one month before Mars Global Surveyor arrives at Mars, then the surface temperature, pressure and opacity measurements will be monitored during the aerobraking phase to provide confirming evidence of dust activity on the surface. The Pathfinder entry profile also provided new and valuable data about the density all the way up to 120 km, which will be used to update the atmospheric models before the start of the Mars Global Surveyor aerobraking phase,

Several Earth based measurements will also be made. The Hubble Space Telescope will take several images of Mars near the start of the aerobraking phase, before Mars gets too close to the Sun as viewed from the Earth. Hubble images taken during the week before the Pathfinder landing showed local dust activity near the Pathfinder landing site, A more quantitative Earth based measurement is made periodically by Dr. Todd Clancy of the Space Science Institute in Boulder, Colorado using the National Radio Astronomy Observatory microwave antenna located at Kitt Peak, Arizona. The global average atmospheric temperature structure can be inferred from the surface to about 60 km by observing the spectrum near one of the Carbon Monoxide absorption lines. Dr. Clancy has been able to infer that moisture in the atmosphere is usually able to confine the dust to lower altitudes, where it has a minimal impact on the densities at higher altitudes. As Mars gets closer to the Sun, the average atmospheric temperature increases, which raises the saturation altitude of water, which allows the dust to reach higher altitudes and have a greater effect on the atmosphere. Previous observations indicate that there is a "Dust Storm Season" which **lasts for several months on either** side of perihelion where there is a much greater chance for global dust storms to develop. The project is spending considerable resources to monitor the atmosphere during the aerobraking phase not only because periapsis must be raised in order to survive the effects of a global dust storm, but also because the aerobraking phase coincides with the first half of the dust storm season.

AEROBRAKING TRAJECTORY MODIFICATIONS

The planned aerobraking trajectory has also been changed to accommodate the lower heating limits with the cell side of one of the panels exposed to the flow. The primary changes include capturing into a smaller period orbit, starting Walkin earlier, using larger Walkin steps and-performing the Walkin maneuvers on consecutive orbits to reach the main phase earlier.

Figure 7 shows how the apoapsis altitude decays due to the drag at periapsis for a recent simulation. The actual baseline will be finalized in early September. Although the ΔV per orbit due to drag is nearly constant at about 5 m/s per orbit during the Main Phase, the amount of apoapsis decrease for a given ΔV decreases as the orbit shrinks, but the daily rate of apoapsis decay remains nearly constant because the number of orbits per day increases as the orbit shrinks.

The horizontal axis for each of the remaining plots is Days Since September 10 (UTC), which was the earliest arrival date at the start of the project, even though the actual arrival date is now September 12. Each plot has a grid of key events near the upper and lower edges. The orbit period is indicated just above the top of the plot. The orbit is nearly face-on to the Sun at the start of aerobraking and nearly face-on to the Earth 60 days later, The start of the first Viking-77 global dust storm started at a longitude of the Sun of about L_s = 200° (Day 40) and may represent the typical starting L_s for Global Dust Storms. Initially, the argument of periapsis of 147° puts periapsis at about 33° North Latitude. As the orbit shrinks, the argument of periapsis decreases at an increasing rate, and periapsis eventually passes the North Pole near the start of the Walkout phase. The atmospheric models indicate that the atmosphere is unusually cold near the North pole. The horizontal bars just below the top edge of the plot indicate several things: when periapsis is over the night side of the planet, when periapsis is eclipsed from the Sun, when periapsis is occulted from the Earth, and the Walkin and Walkout phases. The Walkin phase is where periapsis is lowered in small steps until the desired density is achieved and is needed because the atmospheric density at the aerobraking altitudes is not well known. The Walkout phase is where daily 1.5 m/s propulsive maneuvers are used to maintain a minimum orbit lifetime of 2 days so that there will be sufficient time to recover from an anomaly and raise the periapsis altitude. Note that early on periapsis is on the Nightside of the planet but the face-on geometry puts periapsis close enough to the terminator and high enough above the planet to avoid an eclipse.

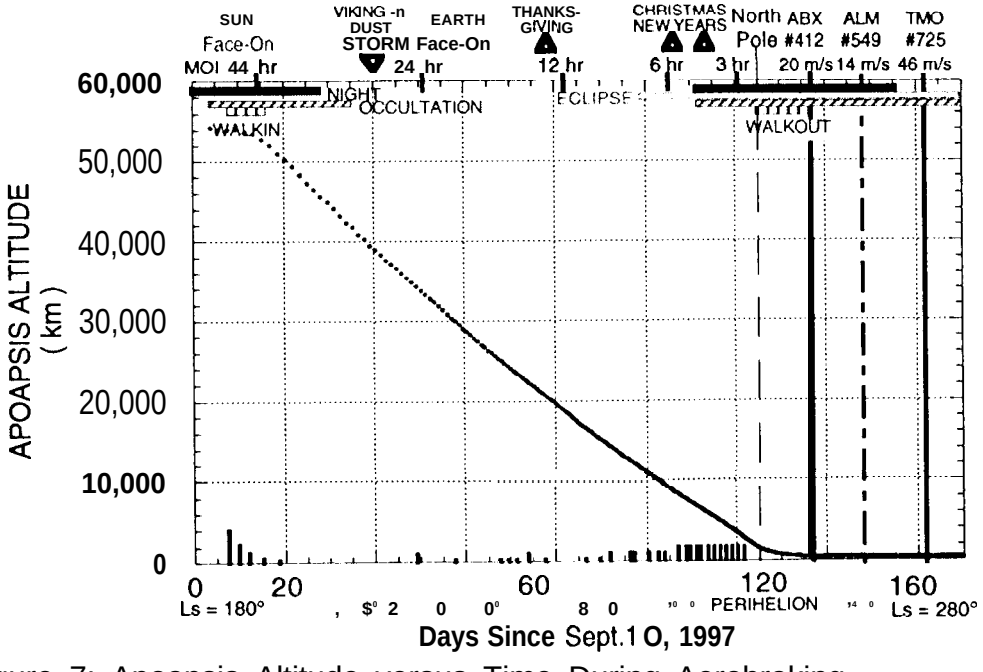

Figure 7: Apoapsis Altitude versus Time During Aerobraking

Figure 8 shows the Periapsis Altitude and includes the Apoapsis Altitude near the end of aerobraking. The capture orbit is targeted to a periapsis altitude of about 300 **km, although the project is considering** a lower target of about 250 km to compensate for the extra propellant that will be used to achieve the smaller capture orbit, The first periapsis (not shown) is Mars Orbit Insertion (MOI). The second periapsis pass is part of the spacecraft checkout orbit where the spacecraft will be in the Array Normal Spin attitude. The third periapsis pass is allocated to contingency science, so the +Z axis of the spacecraft will be pointed at Mars and science data will be collected and recorded for playback later in the orbit. The first Aerobraking Maneuver (AB-1) to lower periapsis to 150 km occurs at the next apoapsis such that the fourth periapsis is the first pass through the sensible atmosphere in the "tail-first" aerobraking configuration.

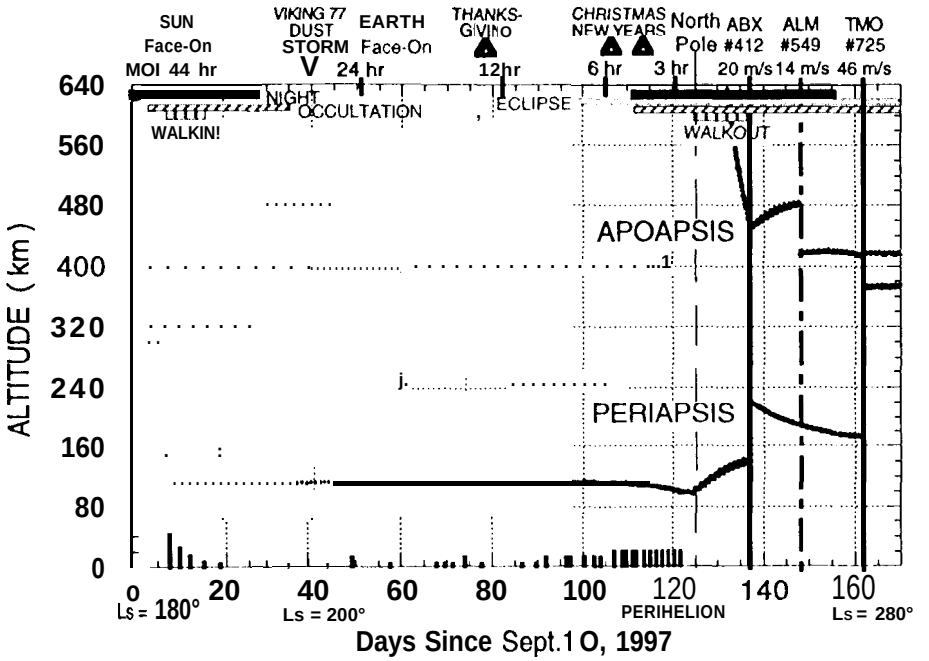

Figure 8: Periapsis Altitude During Aerobraking

The short vertical lines along the bottom axis of the trajectory plots indicate the location and relative magnitudes of all of the Aerobraking trim Maneuvers (ABM's). Although all of these maneuvers lower periapsis in most of the simulations, we expect to use some maneuvers to raise periapsis during actual operations because the real atmosphere is not as well behaved as our atmospheric models[10]. During the Walkin phase, the size of the maneuvers decreases as the spacecraft approaches the desired altitude. Near the end of the Main Phase, where periapsis is approaching the Night side, larger, more frequent maneuvers are required to force periapsis to lower altitudes in order to maintain the required drag because a given density is at a much lower altitude when the atmosphere is cold. Once the orbit lifetime drops below 2 Days, a maneuver is used to raise periapsis enough to add one day of orbit lifetime. This "Walkout"

phase of daily periapsis raise maneuvers begins when the apoapsis is about 2,000 km and continues until ABX, when the apoapsis altitude reaches 450 km.

The Aerobraking Exit (ABX), Apoapsis Lowering (ALM), and Transfer to Mapping Orbit (TMO) maneuvers are indicated by vertical lines toward the right of the plot. The mission plan only describes an ABX to raise periapsis and stop further apoapsis decay, and a TMO to lower apoapsis such that the resulting orbit is the desired mapping orbit. This example trajectory includes an option to collect high resolution gravity data over the South Pole by using ABX to raise periapsis just enough to stop aerobraking rather than all the way up to the mapping orbit altitude. An ALM maneuver to lower apoapsis to an altitude which would naturally drift to the mapping orbit altitude is inserted into the middle of the transition phase. During the transition phase, the argument of periapsis decreases by almost 60/Day. When periapsis reaches the South Pole, the TMO maneuver is used to raise periapsis and lock the spacecraft into a frozen, Sun-Synchronous Mapping orbit.

Figure 9 shows the free stream heating rate at periapsis. The thermal team uses this value, along with the flow and surface accommodation coefficients and the drag duration to compute temperatures at various points on the spacecraft. The thermal team then infers the maximum free stream heating rate that can be tolerated by the spacecraft, The most limiting temperatures are all associated with components on the Solar wings. The curve labelled "90% Design Margin for Atmospheric Blooming" is the design constraint such that if the predicted (or simulated) free stream heating rate is below this 900/. constraint, then the actual **density (or heating) can be almost twice as large as expected without damaging** the spacecraft. Pre-launch estimates of atmospheric variability at 110 km from orbit to orbit were as large as 30% 1-sigma, so a 90% margin was chosen for the trajectory designs. (20°/0 is allocated for Nav and 70°/0 for atmospheric variability). This 90% margin accommodates random fluctuations in the density, but is not large enough to protect the spacecraft from the systematic increase that occurs during a global dust storm. The 90% margin increases as the duration of the eclipse increases near the 6 hour orbit period (Day 100) since the temperatures at the start of the drag pass are lower. The sharp drop in the heating limit near the 3 hour orbit (Day 120) is due to the fact that the duration of the drag pass begins to increase rapidly once the orbit period falls below about 4 hours, so the heat from the collisions with the atmospheric molecules has a longer time to soak in.

Since the cell side of one of the panels is now exposed to the flow, the thermal limit was reduced, which required that the baseline trajectory be redesigned in order to maintain the desired 90% margin for atmospheric variability. Two methods for reducing the planned free stream heating rate at periapsis are to decrease the capture orbit period and to spread the aerobraking phase over a larger number of orbits. The planned capture orbit period was reduced from 48 hours to 45 hours to reduce the energy that must be removed from the trajectory. Arrival was targeted to a lower altitude to increase the effectiveness of the MOI maneuver and partially compensate for the larger AV required to achieve a lower

period following capture. One way to increase the duration of the main phase so that aerobraking could be spread over a greater number of orbits was to move the start of the main phase earlier. Since the optimum arrival date is essentially determined at the time of launch, the only way to start the main phase earlier was to shorten the Walkin phase and start Walkin earlier. One of the two orbits allocated to contingency science before the start of aerobraking was removed, and the drag rehearsal orbit prior to AB-1 was deleted. These changes moved the start of the Walkin phase 4 days earlier. The first several Walkin maneuvers are now planned to occur on consecutive orbits, rather than every other orbit, which moves the end of the Walkin phase another 4 Days earlier. Slightly larger maneuver sizes will be allowed, which may reduce the number of Walkin maneuvers by one. The combined effect of these changes to the trajectory reduced the peak free stream heating rate from 0.35 to 0.28 W/cm*, a 20% reduction.

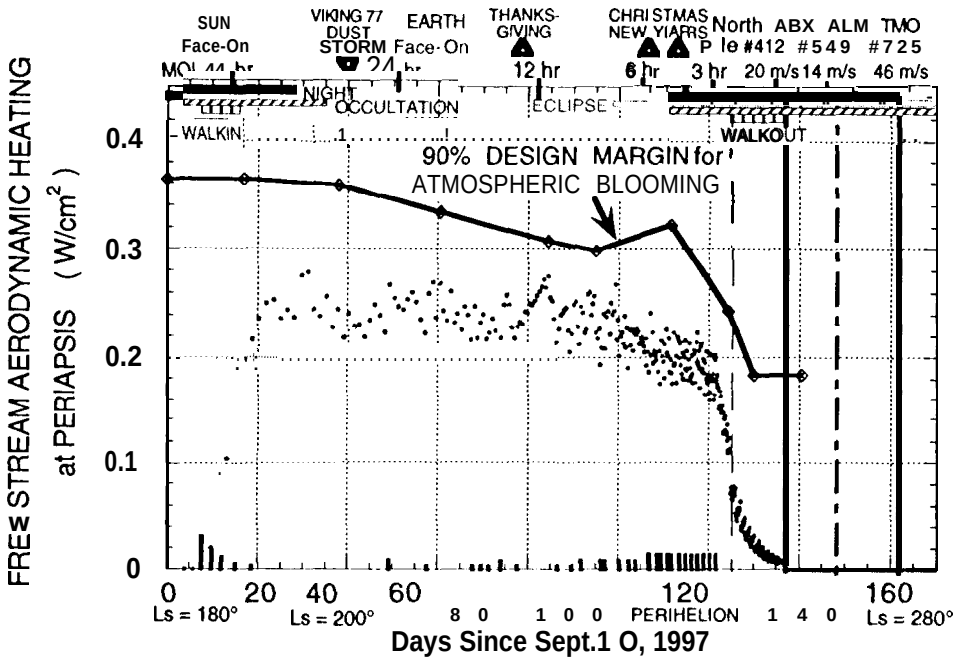

Figure 9: Free Stream Aerodynamic Heating Rate at Periapsis & Constraint

When the plan to hold the panels in position using the gimbal motors was first discussed, the contractually specified maximum gimbal holding torque was the limiting factor in the aerobraking design. The gimbal holding torque put a limit on the maximum Dynamic Pressure. Post-1 aunch tests showed that the holding capability greatly exceeded the contractual requirement, and the thermal limit became the primary design consideration. Figure 10 shows that holding the Dynamic Pressure close to a constant average value with a slight reduction at the end of the Main phase results in a free stream heating rate which tends to follow the shape of the thermal constraint (Figure 9). The scatter in the dynamic pressure and the free stream aerodynamic heating rates in the simulations is due only to the longitudinally dependent gravitational perturbations acting on the orbit. The expected scatter in the atmosphere is not simulated during the trajectory design,

although the heating rate from the design is later compared to the heating rate limits to make sure that the planned trajectory always has at least a 90% margin to accommodate atmospheric variability from orbit to orbit.

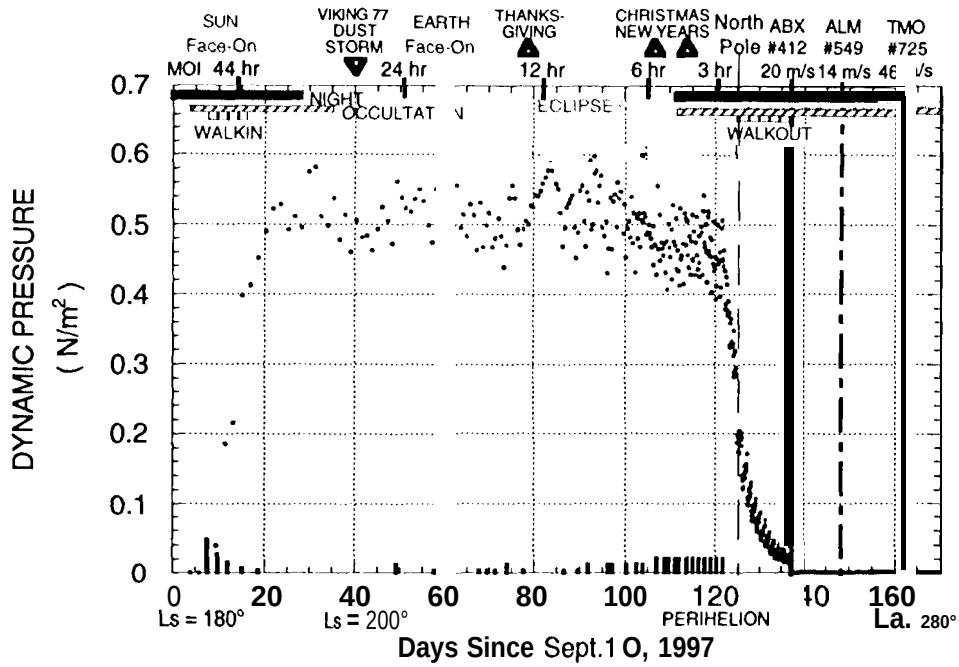

Figure 10: Dynamic Pressure at Periapsis **versus** Time

Achieving a nearly-circular, Sun synchronous orbit with a descending **node at** a Mean Local Solar Time of 2 pm is a requirement from the Project Science Group. Figure 11 shows that the True Local Solar Time for this trajectory continues to decrease, even for the Mapping Orbit which begins at the TMO maneuver. Since Mars is near perihelion at the end of the aerobraking phase, Mars is traveling faster than average, which results in a decreasing True Local Solar Time, even though the Mean Local Solar Time is constant for the mapping orbit. The Mean Local Solar Time for this trajectory actually dips below 14:00 hours (2 pm) during the aerobraking phase but then increases slightly during the last few days of the Walkout phase and during the transition to the mapping orbit. **Since the nodal rate depends on the orbit period and the inclination, using the South Pole Gravity** option with a periapsis altitude two hundred kilometers below the Sun-Synchronous value and an apoapsis less than 40 km above the Sun-Synchronous value means that the orbit period between ABX and TMO is smaller than the Sun-Synchronous value so the nodal rate that is faster than the Sun-Synchronous value and **the Mean Local Solar time gradually increases. The trajectory shown** takes advantage of the increasing Mean Local Solar Time during the transition phase to spread the aerobraking phase over several more orbits than a trajectory which must exit the atmosphere at **exactly 2** pm, and thus lowers the average heating rates and temperatures.

Although the inclination is corrected at ABX in this example trajectory, the Mean Local Solar Time of the final mapping orbit can be fine-tuned by choosing when the inclination is adjusted. Limited propellant margin and the high propellant cost to change the inclination severely limit the ability to control the final Mean Local Solar Time using the inclination because including an out-of-plane inclination correction component with the in-plane component of the ABX or ALM maneuvers drastically reduces the propellant required to correct the inclination. Since the TMO maneuver occurs over the North Pole, adding an out-of-plane component would change the node rather than the inclination.

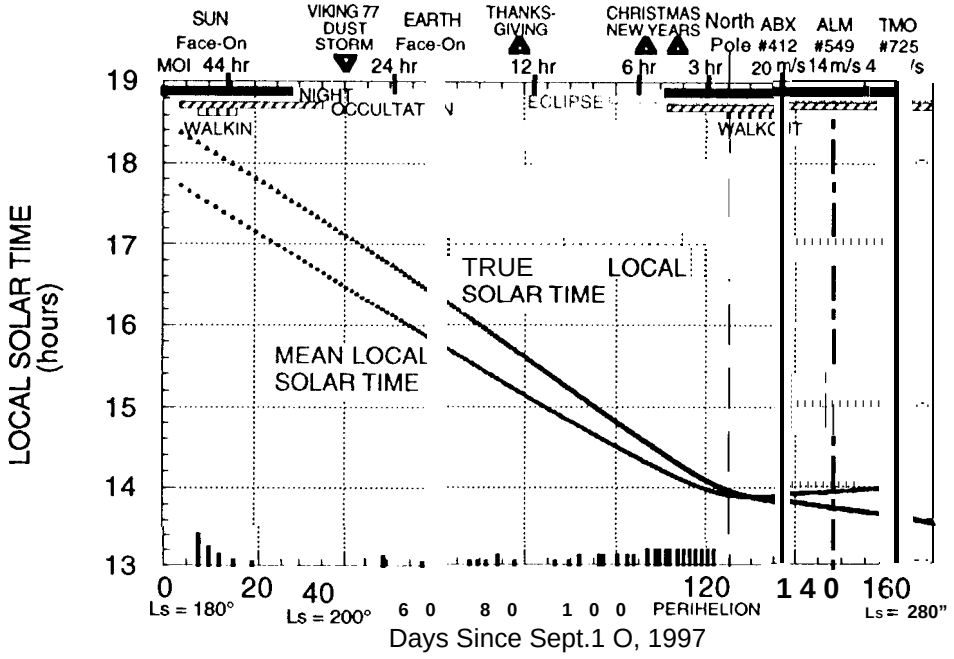

Figure 11: True and Mean Local Solar Time versus Time

Figure 12 shows the inclination for this example trajectory. Note that there is a sharp drop in inclination near the 24 hour gravitational resonance where periapsis flies by the same area on the planet several orbits in a row, which in this case is an area that produces a strong inclination decrease. There are two gravitational "bulges" on opposite sides of Mars[9] that result in a strong decrease in the inclination when periapsis flys **by on one side of the** bulge and a strong increase **in the inclination** when periapsis flys by on the other side of the bulge. **For** example, during the first sharp drop in inclination, every other orbit has the same longitude on the planet as near the 24 hour orbit. Very often there will be either a sharp decrease or a sharp increase near the 12 hour orbit resonance, although for this particular trajectory, periapsis happened to fly through a longitude region where the perturbations cancelled out. The MOI inclination of 93.3° for this example trajectory was chosen to offset the expected change in the inclination during the aerobraking phase due to the gravitational and atmospheric effects. Quite by accident, this particular trajectory ended very close to the 93.0° value

required by the Mapping orbit so very little inclination correction was required at ABX. In fact, the inclination correction at ABX in this example should have been a little larger to account for the perturbations that occurred between ABX and TMO. The most likely scenario is that a crude inclination correction will occur as part of the ABX maneuver, a fine-tuning of the inclination will occur as part of the ALM maneuver, and a final cleanup adjustment will be performed as part of the first Orbit Trim Maneuver (not shown) that is planned for 12 days following TMO. Since correcting the inclination while in the Mapping orbit requires about 6 m/s per tenth of a degree of inclination change, and since the total propellant margin is currently less than 20 m/s, the evolution of the actual inclination during aerobraking will be a closely monitored parameter, especially since the design process occasionally produces a trajectory where the inclination increases by 0.10 or decreases by more than 0.5°.

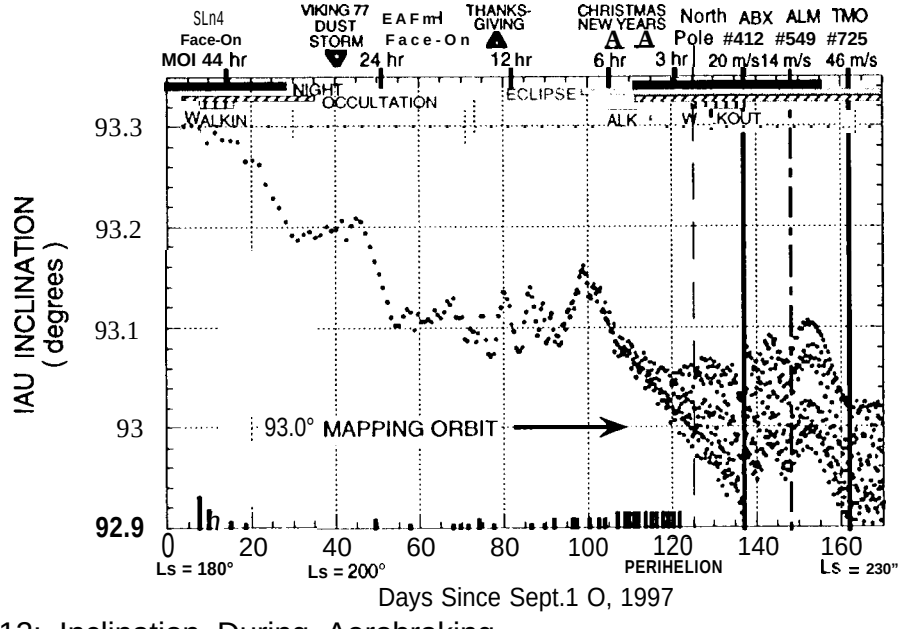

Figure 12: Inclination During Aerobraking

CONCLUSIONS:

The failure of the -Y solar wing to latch up fully during the initial spacecraft deployment challenged the Mars Global Surveyor Operations Team to not only understand the cause of the failure and characterize the response of the unlatched configuration, but also to develop new spacecraft configurations that would be able to survive both the Mars Orbit Insertion maneuver and the aerobraking phase that puts the spacecraft into the orbit that is required to properly map the planet Mars as planned. This paper has described the most probable failure scenario, and the changes that were made to the spacecraft configuration and to the aerobraking trajectory in order to achieve the planned mission objectives in spite of a mission threatening hardware failure.

ACKNOWLEDGMENTS

The work described inthispaper represents notorrly theefforts of the Mars Global Surveyor Operations Team, which is partially located at the Lockheed Martin Astronautics facility **in Denver and also at the Jet Propulsion Laboratory in** Pasadena, but also contributions by many of the original subcontractors. The redesign effort was accomplished in a very short time, in parallel with the normal activities associated with flying a spacecraft by a team that was already extremely small due to the budgetary constraints that currently exist.

Further information about all of the JPL missions, including the Mars Global Surveyor, are available through the World Wide Web at http: //jpl.nasa.gov or the MGS home page at http: //mgsw3.jpl.nasa. gov.

REFERENCES

[1] W. Lee, **and W. Sidney, "Mission Plan for** Mars **Global Surveyor" , AAS/AIAA Flight Mechanics Conference, Austin** TX, Feb. 13-15, 1996, AAS 96-153

[2] J. Beerer, R. Brooks, P. Esposito, D. Lyons, W. **Sidney, H. Curtis & W.** Willcockson, **"Aerobraking at** Mars: **the** MGS Mission", AIAA 34th Aerospace Sciences Meeting , Reno, 1/15-18/96, AIAA 96-0334.

[3] S. Dallas, "The Mars Global Surveyor Mission", 1997 IEEE Aerospace Conference, Snowmass, Colorado

[4] D.T. Lyons, "Aerobraking: The Key to Affordable Mars Exploration", 2nd International Low-Cost Spacecraft Conference, John Hopkins University, Applied Physics Laboratory, Laurel Maryland, USA, April 16-19, 1996, IAA-L-0512

[5] D.F. Rault, "Transitional Flow Effects on Aerodynamics of Mars Global Surveyor During the Aerobraking Maneuver", submitted to the AIAA Thermophysics Conference, New Orleans, LA.

[6] D.T. Lyons, W. Sjogren, W.T.K. Johnson, D. Schmitt, and A. McRonald, "Aerobraking Magellan", AAS/AIAA Astrodynamics Conference, Durango, CO, Aug. 19-22, 1991. AAS-91-420.

[7] D. T. Lyons, D. Griffith, S. Saunders., 'The Magellan Venus Mapping Mission: Aerobraking Operations", 44th Congress of the International Astronautical Federation, Graz, Austria, October 16-22, 1993. paper IAF-93-Q.4.409

[8] D.T. Lyons, "Aerobraking Magellan: Plan versus Reality", AAS/AIAA Spaceflight Mechanics Meeting, Cocoa Beach, FL, February 14-16, 1994. AAS 94-118.

[9] A.S. Konopliv and W.L. Sjogren, "The JPL Mars Gravity Field, Mars50c, Based Upon Viking and Mariner 9 Doppler Tracking Data", JPL Publication 95-5, Feb. 1995.

10 C. G. Justus, "Mars Global Reference Atmospheric Model for Mission Planning and Analysis", *Journal of Spacecraft and Rockets,* Vol. 28, No. 2, March-April 1991, pp. 216-221.